# Atomistic Simulations for Understanding Microscopic Mechanism of Resistive Switches


**S. Watanabe and B. Xiao**

**Abstract** In this chapter, we describe the results of our first-principles simulations to investigate the switching mechanism of amorphous $TaO_x$ (a-$TaO_x$) based resistive switching devices. For the Cu/a-$Ta_2O_5$/Pt atomic switch, we first discuss the atomic structure of the conductive filaments, focusing on the exploration of possible thinnest filament structure. Then we discuss the structures of interfaces between metal electrodes and a-$Ta_2O_5$, which are important in understanding Cu ion supply for the switching. For the Pt/a-$TaO_x$/Pt resistive switch, we discuss the nature of the conductive filaments and diffusion behaviors of active ions. Here we point out the importance of Ta-Ta bonding and the non-negligible contribution of Ta diffusion under certain conditions.

## 1 Introduction

The resistive switches based on metal oxide have got wide attention because of their excellent retention, long endurance and low power consumption. Such devices are composed of an insulator layer ($HfO_x$, $TiO_x$, $TaO_x$, *etc*.) between two electrodes [1–3]. On the basis of different switching behaviors, the devices could be divided into the following two categories: (1) unipolar switches (such as Pt/$TaO_x$/Pt), where the insulator material is sandwiched between two inert electrodes [4], and the switching is realized by changing the magnitude of the applied electric field with keeping its polarity; (2) bipolar switches (including the atomic switches such as Cu/$Ta_2O_5$/Pt), which have asymmetric structures with inert and oxidizable electrodes [5], and change their states by applying the electric fields with different polarities.

S. Watanabe (✉)
Department of Materials Engineering, The University of Tokyo, Tokyo, Japan
e-mail: watanabe@cello.t.u-tokyo.ac.jp

B. Xiao
School of Chemistry and Chemical Engineering, Yantai University, Yantai, China



M. Aono (ed.), *Atomic Switch*, Advances in Atom and Single Molecule Machines,
https://doi.org/10.1007/978-3-030-34875-5_6

Among the oxide-based resistive switching devices, those including amorphous-$TaO_x$ (a-$TaO_x$) were widely studied, which exhibit excellent performance [3–5]. In general, the switching of these devices could be attributed to the forming/rupture of conduction filaments (CFs). However, the atomistic details of switching mechanisms of a-$TaO_x$-based resistive switches has been unclear until recently. More specifically, (1) in a-$TaO_x$-based bipolar switches such as Cu/a-$Ta_2O_5$/Pt, the component of CF had been experimentally identified to be Cu [5], while the atomic structure of CF was unclear: the ionization of interface Cu had been found to be the rate-limiting step during the switching process of the device, while the detail atomic structure near the interface region was still unknown, too [5]. (2) In the Pt/a-$TaO_x$/Pt resistive switch, the atomic component of CF, that is, whether it consists of O vacancies or Ta clusters, was still unknown [4]; on the other hand, how the active ions (such as O and Ta) diffuse in a-$TaO_x$ was also unclear.

We tackled with the above issues via first-principles simulations based on the density functional theory (DFT) [6–11]. In this chapter, we discuss the atomic structures of the CFs, the interface structures, and the diffusion behaviors of active ions in a-$TaO_x$-based resistive switching devices on the basis of our simulation results.

## 2 Computation Methods and Models

### *2.1 Methods*

The calculation of structure relaxation, electronic properties and molecular dynamics (MD) simulations were carried out using the Vienna ab initio simulation package (VASP) [12, 13]. The projector augmented-wave (PAW) [14] method and the generalized gradient approximation (PW91) [15] were adopted to describe the atomic core electrons and electron-electron interactions, respectively.

The calculations of electronic transport properties were carried out via the Atomistix Tool-kit (ATK) program [16]. A numerical atomic basis set, a single-ζ basis with polarization, was used to solve the Kohn–Sham equations. The Perdew-Burke-Ernzerhof (PBE) functional form within the generalized gradient approximation (GGA) was adopted for electron-electron interaction [11].

### *2.2 Structure of Amorphous $Ta_2O_5$*

In real tantalum-oxide-based resistive switching devices, $TaO_x$ is always in the amorphous phase. Therefore, we performed most of our simulations assuming the amorphous $TaO_x$ (a-$TaO_x$) phase. We first built an a-$Ta_2O_5$ (i.e. a-$TaO_{2.5}$) structure by melt-quenching method using VASP. More specifically, the initial crystalline δ-$Ta_2O_5$ structure was melted by MD simulation at 6000 K for 9 ps, and

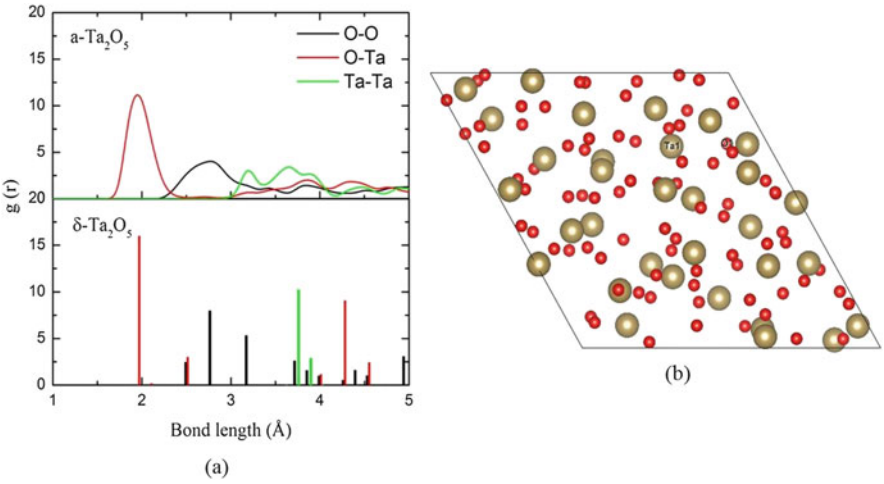


**Fig. 1** (**a**) Partial pair correlation functions of amorphous and crystal $Ta_2O_5$ (reproduced from Ref. [6]) and (**b**) the top view of the a-$Ta_2O_5$ structure

subsequently quenched down to room temperature (300 K) with the rate of 4 K/3 ps. After that, the as-generated amorphous structure was further equilibrated at room temperature for 9 ps.

The amorphous model generated in this way has the following structural features [6]. As seen in the calculated partial pair correlation functions of amorphous and crystalline $Ta_2O_5$ (Fig. 1a), the first peak in a-$Ta_2O_5$ is located at 1.93 Å, which corresponds to the O-Ta bond length and is similar to that in δ-$Ta_2O_5$. On the other hand, the bond length of Ta-Ta (3.20 Å) in a-$Ta_2O_5$ is shorter than that in δ-$Ta_2O_5$ (3.67 Å), which is attributed to the existence of considerable $Ta_2O_2$ quadrangle units in a-$Ta_2O_5$.

Next, we pay attention to the coordination numbers (CNs) of Ta and O atoms in a-$Ta_2O_5$. Here, a pair of Ta and O is regarded as bonded when their interatomic distance is less than the sum of the covalent radii plus a tolerance factor of 0.10 Å, with the covalent radii of Ta = 1.70 Å and O = 0.73 Å. As for Ta atoms, their first shell is coordinated with O atoms by the formation of octahedral $TaO_6$ and pyramidal $TaO_5$ units with their ratio of 20:9. In the case of O atoms, both $OTa_3$ and $OTa_2$ structures could be found, with their ratio of 25:55. It should be emphasized that these structural parameters, bond lengths and CNs, agree with the previous theoretical and experimental studies [12–14], indicating the reliability of the a-$Ta_2O_5$ structure obtained in our studies. In addition, we have also examined the effects of quenching speed on the structure of a-$Ta_2O_5$. It was found that the structural parameters of a-$Ta_2O_5$ only slightly change with the quenching rate among 4/3 K/fs, 2/3 K/fs, and 1/3 K/fs [6].

Using this a-$Ta_2O_5$ model, we have explored the atomic structures of CFs in Cu/a-$Ta_2O_5$/Pt and Pt/a-$TaO_x$/Pt resistive switches [6, 7], the interface structures of Cu/a-$Ta_2O_5$ and Pt/a-$Ta_2O_5$ [8], and the diffusion behaviors of metal and O ions in a-$TaO_x$ [9–11].

# 3 Switching Mechanism of Cu/a-$Ta_2O_5$/Pt Atomic Switch

## *3.1 Conduction Path in Cu/a-$Ta_2O_5$/Pt Atomic Switch*

The widely accepted switching mechanism of the atomic switch is the formation/rupture of a metal atomic bridge in the insulator between the two electrodes, which has been identified in experiments [17–19]. In the case of the a-$Ta_2O_5$-based atomic switch, composition analyses of a-$Ta_2O_5$ film before and after applying a voltage show that Cu ions migrate from the Cu electrode into the a-$Ta_2O_5$ film, which agrees well with the speculation of the formation of a conducting Cu filament in a-$Ta_2O_5$. On the other hand, previous studies in our group have shown that a conduction channel is formed in the crystal $Ta_2O_5$ film via interstitial Cu atoms, but not via oxygen vacancies [20, 21]. However, it is desirable to examine the case of a-$Ta_2O_5$ since, as mentioned before, the amorphous phase is usually adopted in experiments and prototype devices [12, 13].

### 3.1.1 Single Cu Atomic Chains in a-$Ta_2O_5$

In our study to explore the possible conductive paths in the a-$Ta_2O_5$ structure [6], both atomic positions and lattice constants of Cu doped a-$Ta_2O_5$ structures were fully relaxed. Keeping the previous studies using the Cu-doped crystalline $Ta_2O_5$ [20, 21] in mind, we examined both alternate Ta-Cu atomic chain and continued Cu atomic chain as the candidates of conductive path in a-$Ta_2O_5$ via interstitial Cu atoms or substituting O by Cu atoms. After structural optimization, both the alternate Ta-Cu and continued Cu atomic chains were found in a-$Ta_2O_5$ via substituting O with Cu atoms as shown in Fig. 2a,b. The analysis of the density of states (DOS) indicates the formation of conductive, delocalized defect states near the Fermi level, which can serve as conductive paths. However, both structures were easily destroyed after MD simulations at 500 K. Cu atoms prefer bonding together to single atomic chain arrangements, and tend to form cluster or nanowire structures. This gives us a hint for the formation of Cu filaments in a-$Ta_2O_5$.

### 3.1.2 Cu Nanowires in a-$Ta_2O_5$

Cu structures with bigger diameters such as Cu nanowires have been extensively studied both theoretically and experimentally in environments other than the a-$Ta_2O_5$ matrix [22, 23]. In the present studies [6], two relatively thin Cu nanowires with the interlaced trigonal and tetragonal packing were chosen to be inserted into the a-$Ta_2O_5$ along c-axis (perpendicular to the a-b plane in the unit cell). Although the structures of these two Cu nanowires changed in some degree after structural relaxation, the continued Cu-Cu bonding structures were still observed, and the subsequent MD simulations further confirm their stability. However, we should note

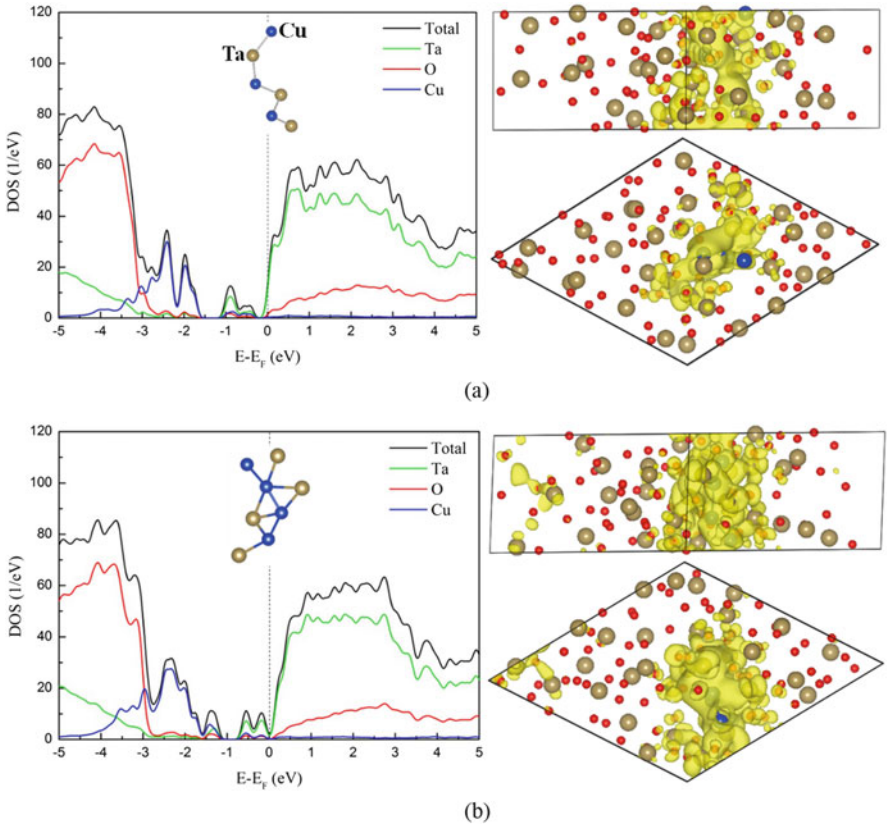


**Fig. 2** Density of states (adapted from Ref. 6) and local density of states near the Fermi level of a-$Ta_2O_5$ with (**a**) alternate Ta-Cu and (**b**) continued Cu-Cu atomic chains

that MD simulations may be insufficient to confirm their stability due to the short time scale compared with that in the practical use. Thus, we also examined their thermodynamic stability, by evaluating the insertion (formation) energies of both structures [6]. The calculated values of insertion (formation) energies are −0.45 (0.48) and −0.29 (0.54) eV, respectively, which suggests that (1) such thin Cu filaments could be stable in a-$Ta_2O_5$, while (2) the Cu atoms in thin filaments are less stable than that in the bulk system. It should be noted that the Cu nanowire structures have been widely observed in experiments [23], even though they are less stable than the Cu bulk system. Thus, we can expect that both of the structures (Fig. 3a,b) can exist in a-$Ta_2O_5$ for sufficiently long periods.

Next, we examine the electronic properties of the Cu nanowires inserted in a-$Ta_2O_5$. In the local density of states near the Fermi level shown in Fig. 3a,b, the conductive paths could be clearly observed. Our projected DOS analyses reveal that the defect states are mainly ascribed to the Cu atoms or Cu-Cu bonding structures.

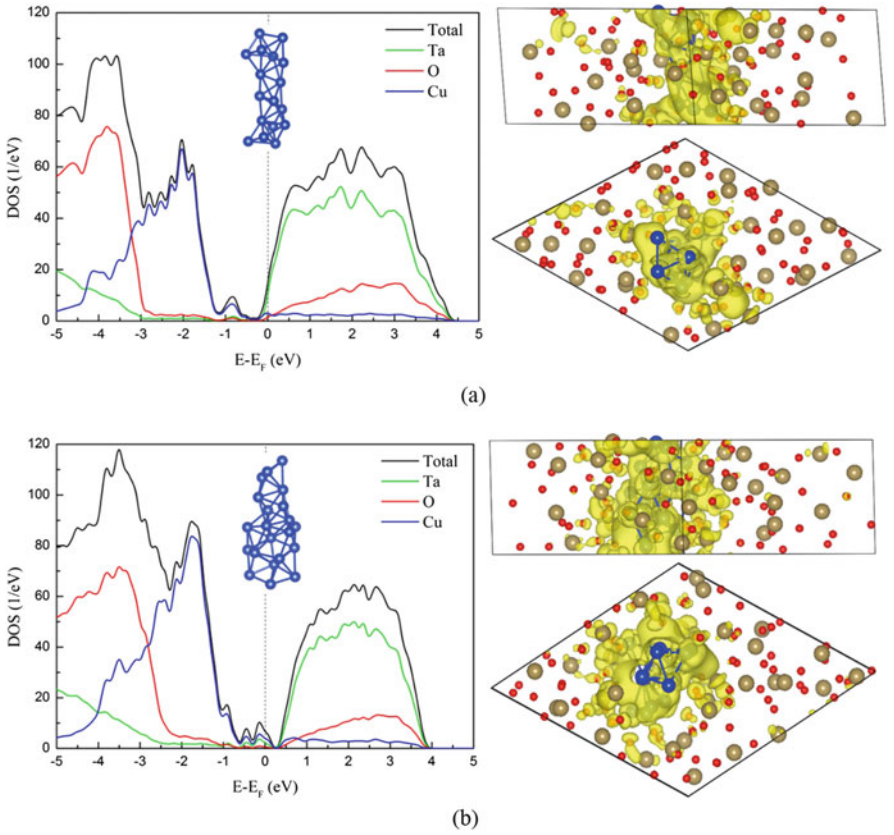


**Fig. 3** Density of states (adapted from Ref. 6) and local density of states near the Fermi level of a-$Ta_2O_5$ with interlaced (**a**) trigonal and (**b**) tetragonal packed nanowires

Thus, we can say that the conduction in the a-$Ta_2O_5$-based atomic switch is ascribed to the formation of continued Cu-Cu bonding.

### 3.1.3 The Thinnest Cu Filament in a-$Ta_2O_5$

Nowadays, downscaling of nanodevices becomes more and more challenging due to physical limitations and increasing processing complexity. So we have explored the thinnest Cu filament that could exist in the a-$Ta_2O_5$, which would be helpful in downscaling of the Cu/$Ta_2O_5$/Pt atomic switch. For this purpose, the following scheme was adopted: starting from the a-$Ta_2O_5$ structure containing a thick Cu nanowire (Fig. 3a), some of Cu atoms were removed from the system each time, and the MD simulation at room temperature and structure relaxation were carried out after each removal step. The removal process was continued until the Cu filament becomes disconnected in a-$Ta_2O_5$. As can be seen in Fig. 4, the thinnest Cu filament generated in this way is composed of the three-membered ring structures with linear

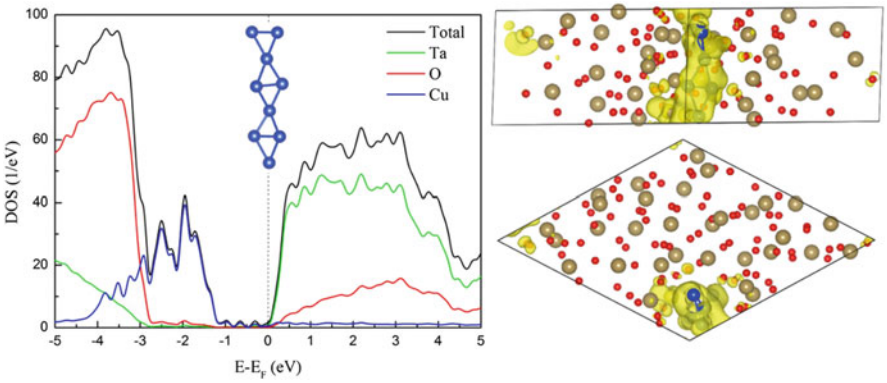


**Fig. 4** Density of states (reproduced from Ref. [6]) and local density of states near the Fermi level of a-$Ta_2O_5$ with the thinnest Cu nanowire in a-$Ta_2O_5$

arrangement. The formation energy of this Cu filament in a-$Ta_2O_5$ is 0.38 eV per supercell. The DOS and partial charge density analyses (Fig. 4) reveal that the thinnest Cu filament is conductive, which agrees well with the "Cu-Cu bonding" conductive mechanism mentioned above.

### 3.1.4 Cu Filament in a-$Ta_2O_5$ with Nanopore

Experimental studies suggest that a-$Ta_2O_5$ films sputtered at room temperature generally have nanoporous structures consisting of piled or small grains, and Cu ions are most likely to migrate along the grain boundaries than inside the grains due to the relatively low migration barriers at the former [5]. Thus the Cu filament is most likely to be formed inside the nanopores. Meanwhile, we would like to emphasize that the atomic density of Cu in our previous calculations is rather high, and it is necessary to investigate the a-$Ta_2O_5$ structure with low Cu concentration. Accordingly, a big stoichiometric a-$Ta_2O_5$ with a nanoporous structure (a-$Ta_{124}O_{310}$) was constructed based on the previously constructed a-$Ta_2O_5$ model (i.e. the model used in the studies of the previous subsections). In this case, most of Ta atoms near the sidewall of nanopore are unsaturated with the O coordination numbers of only 4 or 5. Subsequently, a thicker Cu nanowire with interlaced centered-hexagon packing was inserted into the nanopore. After structural optimization, the conductive path was clearly observed on the Cu filament as shown in Fig. 5. The defect states near the Fermi level have the contributions from both Cu and Ta atoms, indicating the existence of certain Ta-Cu bonds on the sidewall of Cu filaments. It should be noted that in this case (Fig. 5), DOS around the Fermi level are more delocalized as compared with all the others in the present studies due to the increased thickness of Cu filaments. In fact, the increase of number of conduction channels with the increase in the thickness has been reported for isolated Cu nanowires and Cu nanowires encapsulated in a boron nitride nanotube [24]. So we predict that the thick Cu filament is more conductive than the others.

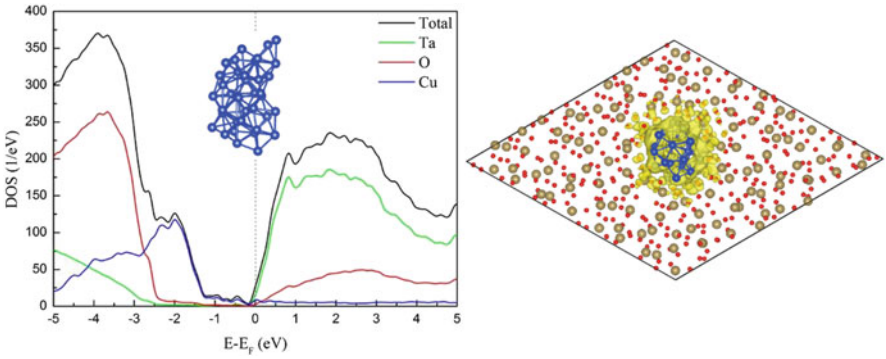


**Fig. 5** Density of states (DOS) and local density of states near the Fermi level of a-$Ta_2O_5$ with the interlaced centered-hexagon packed Cu nanowire in a-$Ta_2O_5$

It is also worth mentioning that the insertion (formation) energy of Cu filament in a-$Ta_2O_5$ (Fig. 5) is −0.94 (−0.46) eV. Accordingly, we can say that the thick Cu nanowire structure in a-$Ta_2O_5$ is thermodynamically stable.

### 3.1.5 Transport Properties of Cu/a-$Ta_2O_5$/Pt with and Without Cu Filament

Next, we examine the electronic and transport properties of Cu nanowires in the Cu/a-$Ta_2O_5$/Pt heterostructure shown in Fig. 6 [6]. We can see that the electron conduction in Cu/a-$Ta_2O_5$/Pt heterostructure is poor due to the insulating nature of a-$Ta_2O_5$. On the other hand, the electron conduction is enhanced by inserting the Cu filament in the a-$Ta_2O_5$ between two Cu and Pt electrodes as seen in Fig. 6c. In addition, when a thicker Cu nanowire with the interlaced centered-hexagon packing is used as the conductive filament, the transmission coefficient further increases (Fig. 6d), which agrees with the thickness dependence of the conduction in Cu nanowires [24]. It is also worth noting that the Cu/a-$Ta_2O_5$/Pt with a discontinued Cu filament (Fig. 6b) has smaller conduction than those with the Cu filaments bridging two electrodes.

In summary of this subsection, we have examined the structure of conduction filaments (CFs) in the Cu/a-$Ta_2O_5$/Pt resistive switch from first principles. Our results reveal that Cu nanowires with various diameters are stable in the a-$Ta_2O_5$ and can serve as CFs. In this case, the Cu-Cu bonding mainly contributes to the conductive, delocalized defect states.

## *3.2 Interface Structures of Cu/a-$Ta_2O_5$/Pt*

In the widely accepted switching mechanism of the Cu/a-$Ta_2O_5$/Pt resistive switch [17–19], there are three main processes: (1) the ionization of Cu at the Cu/a-$Ta_2O_5$ interface, (2) the migration of Cu ions through the a-$Ta_2O_5$ layer, and (3) the

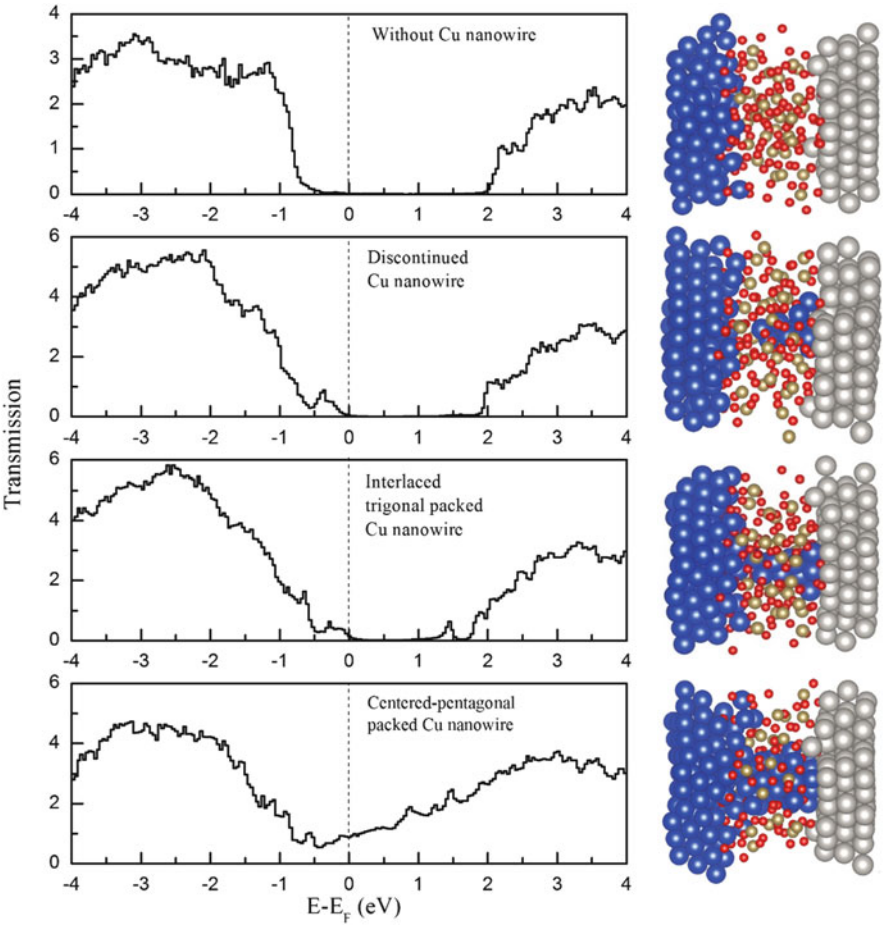


**Fig. 6** Transmission spectra and the corresponding structures for the Cu/a-$Ta_2O_5$/Pt with and without the Cu filament between two electrodes (adopted from Ref. [6])

precipitation of Cu on Pt electrode [5]. The initial ionization of Cu atoms in the Cu/a-$Ta_2O_5$ interface is important in the performance of the switch, in the sense that the ionized Cu atoms are the main source of Cu ions used in the subsequent processes.

Considering the above, in this subsection, we pay attention to the interface structures and electronic properties of Cu/a-$Ta_2O_5$/Pt heterostructure, and their dependence on the interface O concentration and temperature [8].

### 3.2.1 Interface Structures and Electronic Properties of Cu/a-$Ta_2O_5$/Pt Structure

To deepen the understanding on the structural features near the interface between Cu (or Pt) and a-$Ta_2O_5$, three types of Cu/a-$Ta_2O_5$/Pt heterostructures were constructed:

their chemical compositions in the supercell are $Cu_{108}Ta_{32}O_{80}Pt_{84}$, $Cu_{108}Ta_{32}O_{88}Pt_{84}$ and $Cu_{108}Ta_{32}O_{96}Pt_{84}$, and hereafter they are denoted as a-O8, a-O12 and a-O16, respectively. These three models have different interface O concentrations: a-O8 represents the initial Cu/c-$Ta_2O_5$/Pt structure with a stoichiometric c-$Ta_{32}O_{80}$ slab between two electrodes, where O layers of both Cu/c-$Ta_2O_5$ and Pt/c-$Ta_2O_5$ interfaces contain 8 O atoms; In the a-O12 and a-O16 models, extra 4 and 8 O atoms are introduced into each interface, respectively. In preparing the above simulation models, Cu/crystal (c)-$Ta_2O_5$/Pt heterostructures were first constructed with corresponding amounts of interface O atoms, and melt-quenching cycle was performed to generate a-$Ta_2O_5$ layers with fixing the positions of atoms in the electrodes. Then the obtained Cu/a-$Ta_2O_5$/Pt heterostructures were further equilibrated at room temperature (unless otherwise described), which was followed by the structural optimization with relaxing all the atoms.

The as-generated three Cu/a-$Ta_2O_5$/Pt heterostructures are shown in Fig. 7a–c. In the stoichiometric case (a-O8, Fig. 7a), we can see the accumulation of O atoms near the Cu/a-$Ta_2O_5$ interface with forming Cu-O bonds and their depletion near the Pt/a-$Ta_2O_5$ interface where a considerable number of Pt-Ta bonds are found. Most of Cu atoms at the Cu/a-$Ta_2O_5$ interface are connected with single O atom. Their Cu-O bond length is about 2.15 Å in average, which is longer than that in the bulk $Cu_2O$ (1.85 Å). According to the Bader charge analyses (Fig. 8a), the ionization of Cu atoms at this interface occurs with the charge transfer from Cu to O atom of about 0.2e in average. Some Cu atoms at the interface are significantly ionized with forming two Cu-O bonds, accompanied by the charge transfer from Cu to O about 0.4e. Interestingly, these Cu atoms tend to diffuse into a-$Ta_2O_5$ bulk layer. On the other hand, as seen in Fig. 8a, the charge transfer occurs from Ta to Pt atoms at the Pt/a-$Ta_2O_5$ interface by forming Ta-Pt bonds. This Ta-Pt bond formation involves the decrease in the number of Ta-O bonds from $TaO_5$ to $TaO_4$, which results in the reduction of Ta atoms.

As the O content at the interface region increases, the interface structures of Cu/a-$Ta_2O_5$ show larger distortion as seen in Fig. 7b (a-O12) and 7c (a-O16). Interestingly, Ta-O-O bonding structures are seen at the interface region due to the high interface O content, and the O ions in Ta-O-O bond hold less amount of electrons than the others, as can be seen in the Bader charges in a-O16 model (Fig. 8b). It is worth noting that a similar Ta-O-O bonding structure has been identified in Cu/a-$Ta_2O_5$/Pt atomic switch in experiment [25]. It is also noted that, in the a-O12 and a-O16 structures, considerable amount of Cu atoms at the Cu/a-$Ta_2O_5$ interface have diffused into the a-$Ta_2O_5$ bulk region with forming two (predominant) or three Cu-O bonds. The corresponding Cu-O bond length is about 1.90 Å in average, which is a little longer than that in bulk $Cu_2O$ (1.85 Å). For example, in the a-O16 structure, the Cu atoms at the interface region are oxidized with losing about 0.55 electrons in average (Fig. 8b). Since the Bader charge values in the Cu/a-$Ta_2O_5$/Pt systems are about half of the corresponding formal values (for example, the Bader charges of Ta and O atom are about +2.5 and −1e, respectively, while the formal charges are Ta (+5e) and O (−2e) ions in a-$Ta_2O_5$), the Cu atoms at the interface region with 0.55e could be regarded as $Cu^{1.1+}$.

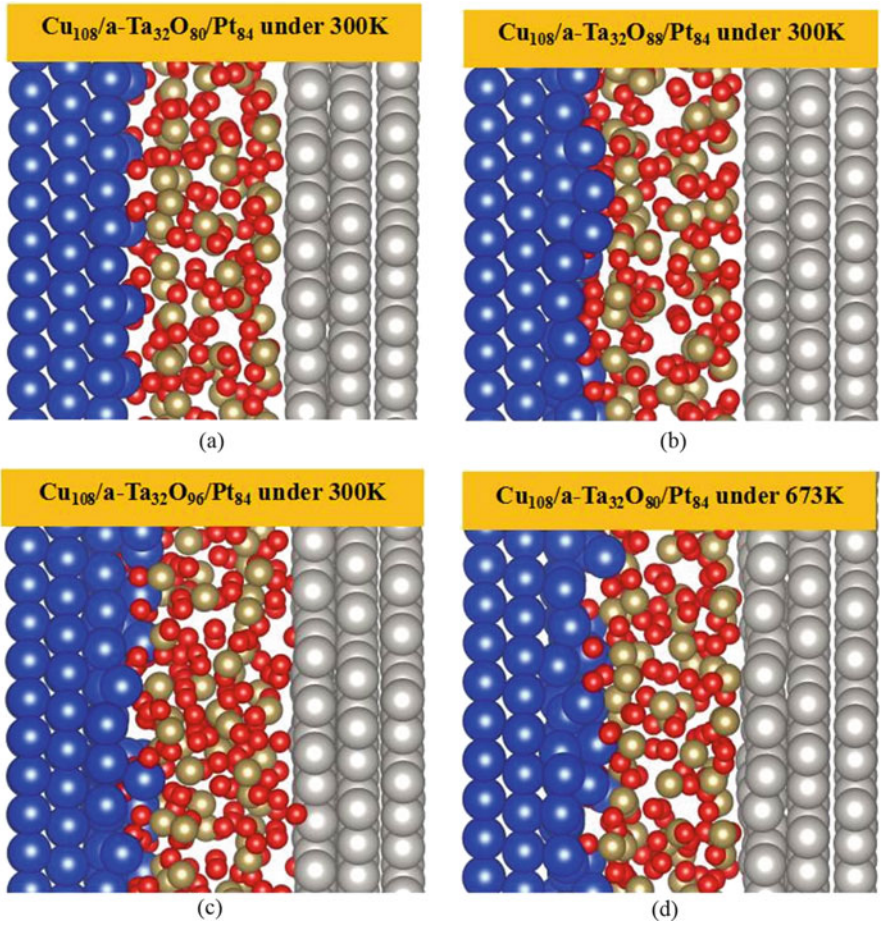


**Fig. 7** Cu/a-$Ta_2O_5$/Pt heterostructures of (**a**) a-O8, (**b**) a-O12, (**c**) a-O16 and (**d**) a-O8 after MD simulations. For the definitions of a-O8, a-O12, and a-O16, see the main text. Reproduced from Ref. [8] with permission from American Chemical Society

For the position of Pt atoms at the interface region, they change only slightly after increasing the interface O content. The Bader charge analyses show that the charge transfers from Pt to O and Ta atoms are about 0.20 and 0.25e, respectively.

Next, we discuss the effect of temperature, because the temperature is considered to be one of the most important factors to affect the switching process of Cu/a-$Ta_2O_5$/Pt device. For example, with the increase of operation temperature, the absolute values of SET voltage of resistive switches gradually decrease [5], which could be partly attributed to the faster diffusion of Cu ions in the devices at high temperature. Meanwhile, the ionization of Cu at the interface region may also be enhanced due to the faster Cu diffusion into the a-$Ta_2O_5$ layer at high temperature. We have examined this point using the a-O8 model. As can be seen in Fig. 7d, the Cu

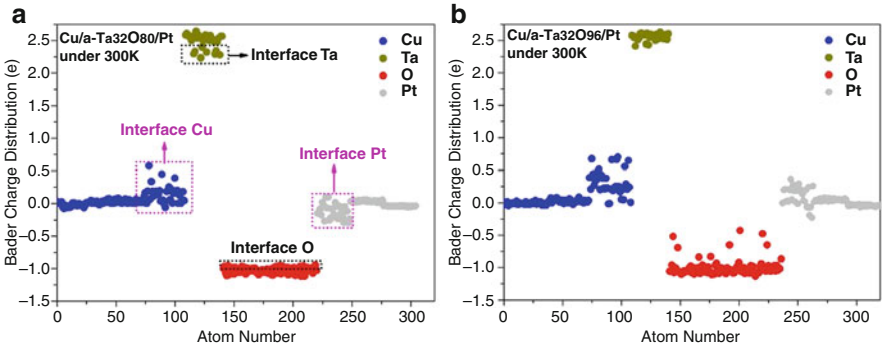


**Fig. 8** Bader charge distributions of (**a**) Cu/a-$Ta_{32}O_{80}$/Pt and (**b**) Cu/a-$Ta_{32}O_{96}$/Pt. Adapted from Ref. [8] with permission from American Chemical Society

atoms at the interface region tend to diffuse into the a-$Ta_2O_5$ layer after 2 ps MD simulation at 673 K, which results in the strong oxidization of these Cu atoms. This confirms that the temperature is one of key factors to control the ionization of Cu atoms at the Cu/a-$Ta_2O_5$ interface.

### 3.2.2 Stability of Cu/a-$Ta_2O_5$/Pt Structure

We next examine the stability of Cu/a-$Ta_2O_5$/Pt structures with various interface O concentrations [8]. Figure 9 shows the interface energies of the a-O8, a-O12 and a-O16 models. It is found that the a-O12 is the most stable among the three within a wide range of O chemical potential. As mentioned before, the content of O at the Cu/a-$Ta_2O_5$ interface is obviously higher than the other regions in the Cu/a-$Ta_2O_5$/Pt structure. In this regard, we predicted that the Cu/a-$Ta_2O_5$ structure with O-rich interface is energetically preferable, where the $Cu_2O$ structure could be found.

Next, we discuss the electronic properties of Cu/a-$Ta_2O_5$/Pt heterostructure. Here, we consider only the a-O12 model for simplicity. As seen in Fig. 10, the DOS of the interface regions is finite around the Fermi level. This means that the interface regions show metallic behavior, and the gap states responsible for this behavior mainly come from the interfacial Cu-O and Pt-O bonding with a very small contribution from the interface Ta atoms as can be seen from Fig. 10. In the central region, on the other hand, both O and Ta atoms have no contribution around Fermi level (see Fig. 10), indicating that the central region of the a-$Ta_2O_5$ is insulating. Thus, the Cu/a-$Ta_2O_5$/Pt interface forms a Schottky contact.

### 3.2.3 Schottky Barrier Height of Cu/a-$TaO_x$/Pt Structure

As we know, the Schottky barrier height (SBH) is the important quantity that should be considered in controlling the initial set bias voltage of Cu/a-$Ta_2O_5$/Pt atomic

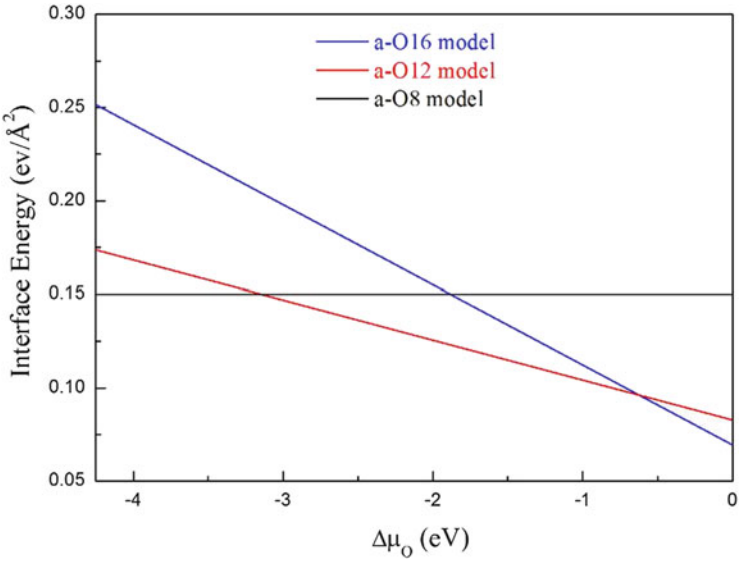


**Fig. 9** Interface energies of a-O8, a-O12 and a-O16 models. Adapted from Ref. [8] with permission from American Chemical Society

switches. In general, SBH could be estimated from the partial density of states (PDOS) as the difference between the Fermi level and valence band maximum (VBM) of the bulk like layer. However, it is difficult to estimate the SBH for our a-$Ta_2O_5$ heterostructures because of their relatively small thickness. In addition, the distribution of macroscopically averaged electrostatic potentials is fluctuant in these heterostructures due to the disordered arrangement of atoms.

Considering the above, we constructed the Cu/λ-$Ta_2O_5$/Pt model with well-defined interfaces. Here the λ-$Ta_2O_5$ is the most stable structure of crystal $Ta_2O_5$ at low temperature [26]. To construct the Cu/λ-$Ta_2O_5$/Pt heterostructure, Cu and Pt (111) surfaces were connected to the (001) surface of λ-$Ta_2O_5$ with O-termination. The lattice mismatch is less than 1%. The corresponding chemical composition of this model is $Cu_{69}/Ta_{36}O_{102}/Pt_{63}$, which is labeled as c-O12 since the λ-$Ta_2O_5$ slab cleaved contains 12 O atoms in the interface layer. Figure 11 shows the PDOS of the Cu/λ-$Ta_2O_5$/Pt models with various O concentrations at the interfaces. From this figure, the SBHs can be obtained as the difference between the Fermi level and VBM in the bulk-like layer. It should be noted that VBM can be more accurately computed than the conduction band minimum within DFT [27]. The estimated p-type SBH is 1.1 eV for the c-O12 case. The large values of p- and n-type SBHs reveal that when the voltage applied to the Cu or Pt electrode is not so large, no conduction channel for the electron flow is formed in this heterostructure.

Next, the SBH in the Cu/λ-$Ta_2O_5$/Pt was calculated as a function of the interface O concentration. In doing so, the corresponding O atoms (from 0 to 50%) were removed from both c-O12 interfaces. As seen in Fig. 11, the PDOS analysis reveals

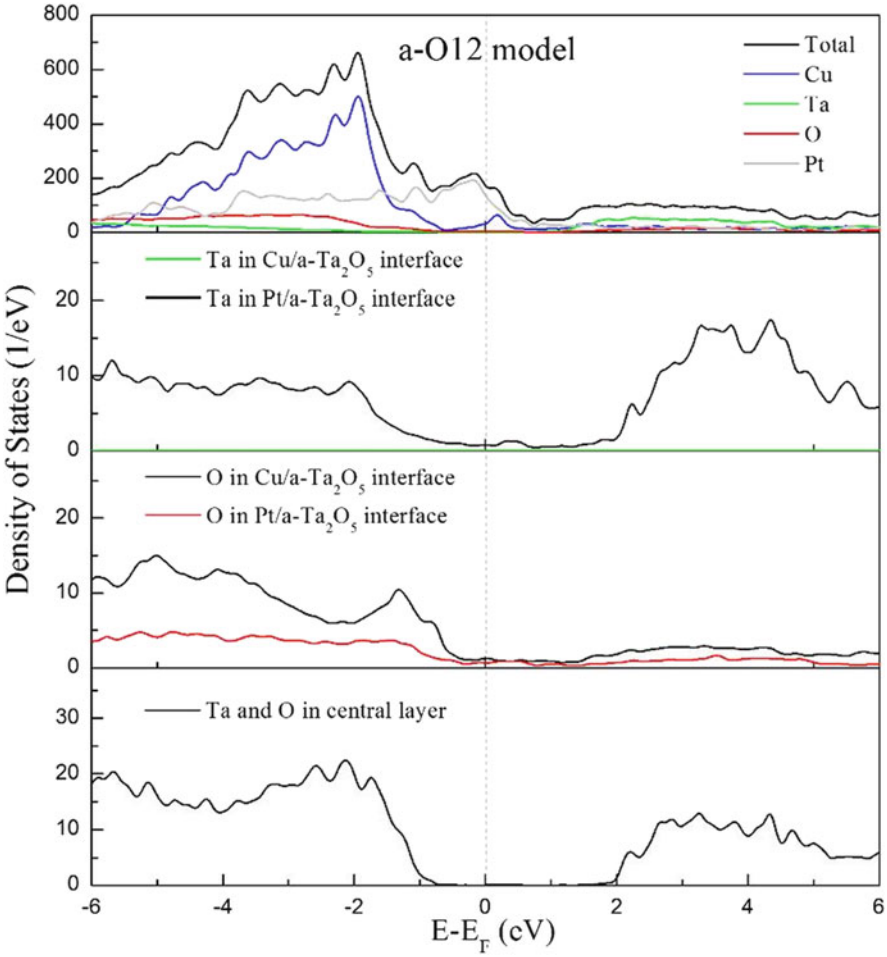


**Fig. 10** Density of states of a-O12 model. Adapted from Ref. [8] with permission from American Chemical Society

that O atoms mainly contribute to the VBM of λ-$Ta_2O_5$, and thus the amount of interface O atoms has a great impact on the VBM of metal oxides. As a consequence, the valance band offset (VBO) increases with the reduction of the amount of interface O atoms, and the VBO can increase up to 1.5 eV by gradually reducing the interface O atoms from 0 to 50%. This increase is attributed to the downward shift of the VBM of $Ta_2O_5$ due to the reduced electronegativity of the total interfacial oxygen as compared to that of the c-O12. Thus, the initial SBH of the Cu/$Ta_2O_5$/Pt atomic switch can be experimentally controlled by tuning the interface O concentration, a property directly related to the ambient oxygen pressure.

In summary of this subsection, we have discussed the interface structures of Cu/a-$Ta_2O_5$/Pt atomic switch. Our results reveal that the Cu atoms tend to be ionized at the

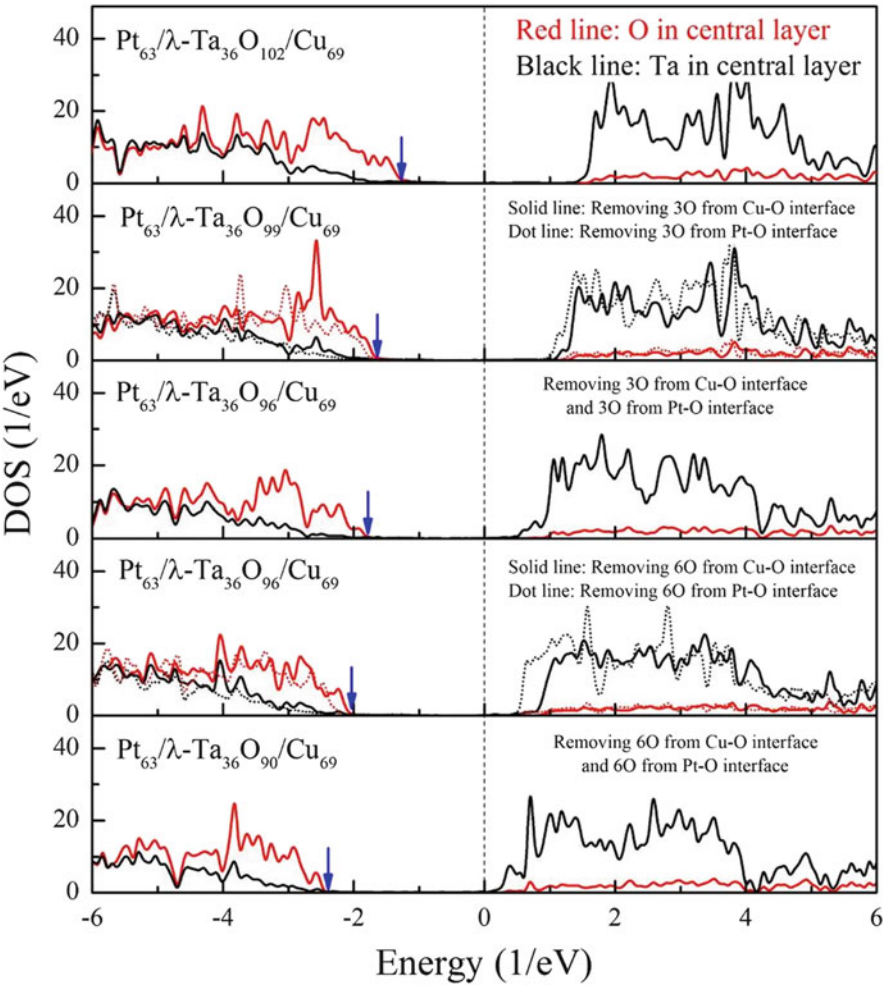


**Fig. 11** Density of States of Pt/c-$Ta_2O_5$/Pt with various interface O contents

interface of Cu/a-$Ta_2O_5$, and the ionization behavior becomes more obvious as the interface O content and/or temperature increases.

## 4 Switching Mechanism of Pt/a-$TaO_x$/Pt Resistive Switch

### *4.1 Conduction Path in Pt/a-$TaO_x$/Pt Resistive Switch*

So far, a-$TaO_x$ ($x < 2.5$) based resistive switches (i.e., Pt/$TaO_{2.5-x}$/$TaO_{2-x}$/Pt) have been extensively studied in the literature and shown superior performance to other

switching materials [28–30]. According to previous reports, the widely accepted switching mechanism of O-deficient-material (such as $TaO_x$ and $TiO_x$) based resistive switches is based on the drift/diffusion of O vacancies ($V_O$s) driven by applied electric fields [31, 32]. In the case of $TiO_x$-based resistive switch, previous experimental and theoretical studies revealed that the conduction filament (CF) is composed of the $V_O$s and the conduction is based on the electron hopping in CF, which causes the negative temperature coefficient of resistance (TCR) in both high resistance state (HRS) and low resistance state (LRS) [32, 33]. Keeping this in mind, several studies explained the switching in the a-$TaO_x$ based resistive switches from the electron hopping conduction and/or the $V_O$-based CF [34, 35]. Recently, Lee et al. [5] and Choi et al. [36] in detail investigated the component of CF in a-$TaO_x$ based resistive switches, and their results show that a considerable amount of continued Ta-rich region ($TaO_{1-x}$) exist in the switching-on state, accompanied by a positive TCR [30, 37]. This implies the strong qualitative difference in the switching behavior between the $TiO_x$ and a-$TaO_x$ systems.

Thus, we examined the origin of switching mechanism in the a-$TaO_x$-based resistive switches via first-principles simulations [7]. Since the switching processes of a-$TaO_x$ based devices strongly correlate with the change of O concentration [5], we examined a-$TaO_x$ structures under various O concentrations to understand the switching mechanism.

### 4.1.1 Structures and Electronic Properties of Single O Vacancies in a-$Ta_2O_5$

Firstly, a stoichiometric a-$TaO_{2.5}$ structure was generated via the melt quenching method. As is well known, the structural and electronic properties of defects are sensitive to their local environments, while the local environments vary site by site in amorphous structures. Therefore, to understand the properties of single $V_O$ in a-$TaO_{2.5}$, all the possible vacancy sites were considered.

As can be seen from Fig. 12a, the stability of vacancy correlates with the Ta-Ta bond length, that is, a structure with a shorter bond length has a lower energy [7]. The length of the Ta-Ta dimer bond formed at the vacancy site is shorter than that in a-$TaO_{2.5}$ (3.20 Å). In particular, the bond length of Ta-Ta dimer (2.84 Å) in the most stable $V_O$ structure is comparable with the one (2.86 Å) in Ta metal. The short bond length suggests good stability of the Ta dimer at $V_O$. To further confirm this, MD simulations were performed at different temperature as shown in Fig. 12b, c. The results reveal that the Ta dimer is very stable at room temperature, while the position of such Ta dimer structure migrates into its adjacent sites at high temperature (i.e., 873 K). Thus, the motion of such a single Ta dimer structure is likely to occur under external electric fields in real devices.

To understand the electronic properties of the $V_O$ in a-$TaO_{2.5}$, we have calculated the DOS for the energetically most stable $V_O$ structure with HSE06 hybrid functional for the exchange-correlation term [38]. The results show that the defect state (mainly coming from $V_O$) appears near the Fermi level, and its location (0.8 eV and 2.5 eV

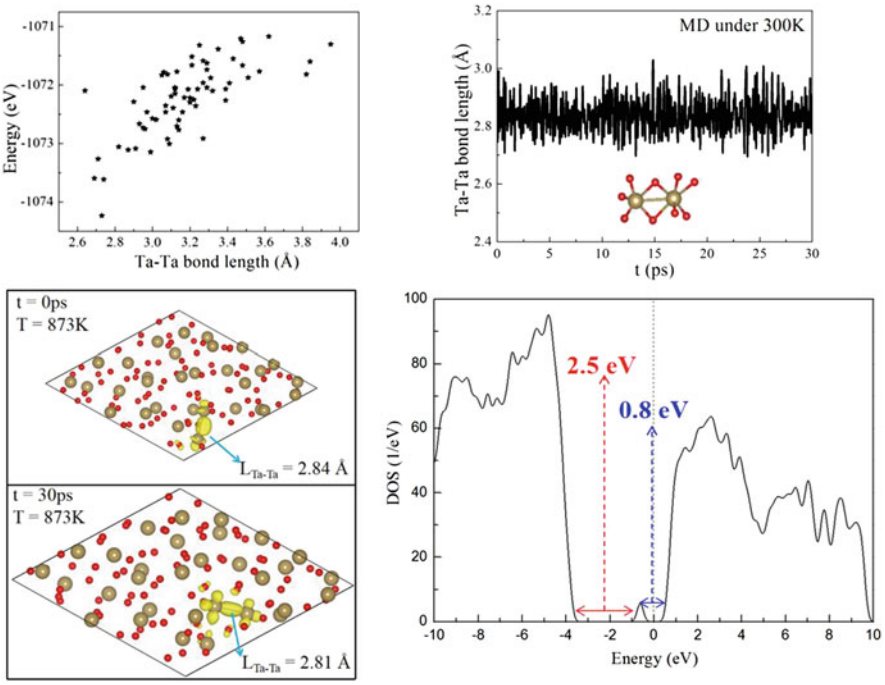


**Fig. 12** (**a**) Relationship between the stability of single O vacancy ($V_O$) and the Ta-Ta bond length at the vacancy site in amorphous $Ta_2O_5$. The change of (**b**) Ta-Ta bond lengths and (**c**) the position of Ta dimer during 30 ps molecular dynamics (MD) simulation. (**d**) DOS of the most stable single $V_O$ structure. Adapted from Ref. [7] with permission from The Royal Society of Chemistry

away from the conduction and valence bands, respectively) agrees with previous experiments [39, 40]. Note that several types of $V_O$ states were found among the 80 single $V_O$ structures in a-$TaO_{2.5}$, which may correspond to the existence of several kinds of current leakage sources in a-$TaO_{2.5}$ capacitor in experiment [41].

### 4.1.2 Structures and Electronic Properties of a-$TaO_{2.5}$ with High $V_O$ Concentration

Next, we consider the a-$TaO_{2.5}$ with high $V_O$ concentration (such as a-$TaO_{2.25}$). The a-$TaO_{2.25}$ structure was generated via melt-quenching method after randomly removing 8 O atoms from the original a-$TaO_{2.5}$ (with 32 Ta and 80 O atoms). In the a-$TaO_{2.25}$, Ta dimer, trimer and tetramer structures coexist as seen in Fig. 13a [7]. The DOS analysis (Fig. 13b) shows the existence of defect states in the band gap region, which consist of mainly the components of these Ta clusters. The energy positions of the defect states become deeper with the increase of the size of Ta cluster, indicating the good stability of big Ta clusters. Subsequent MD simulation at

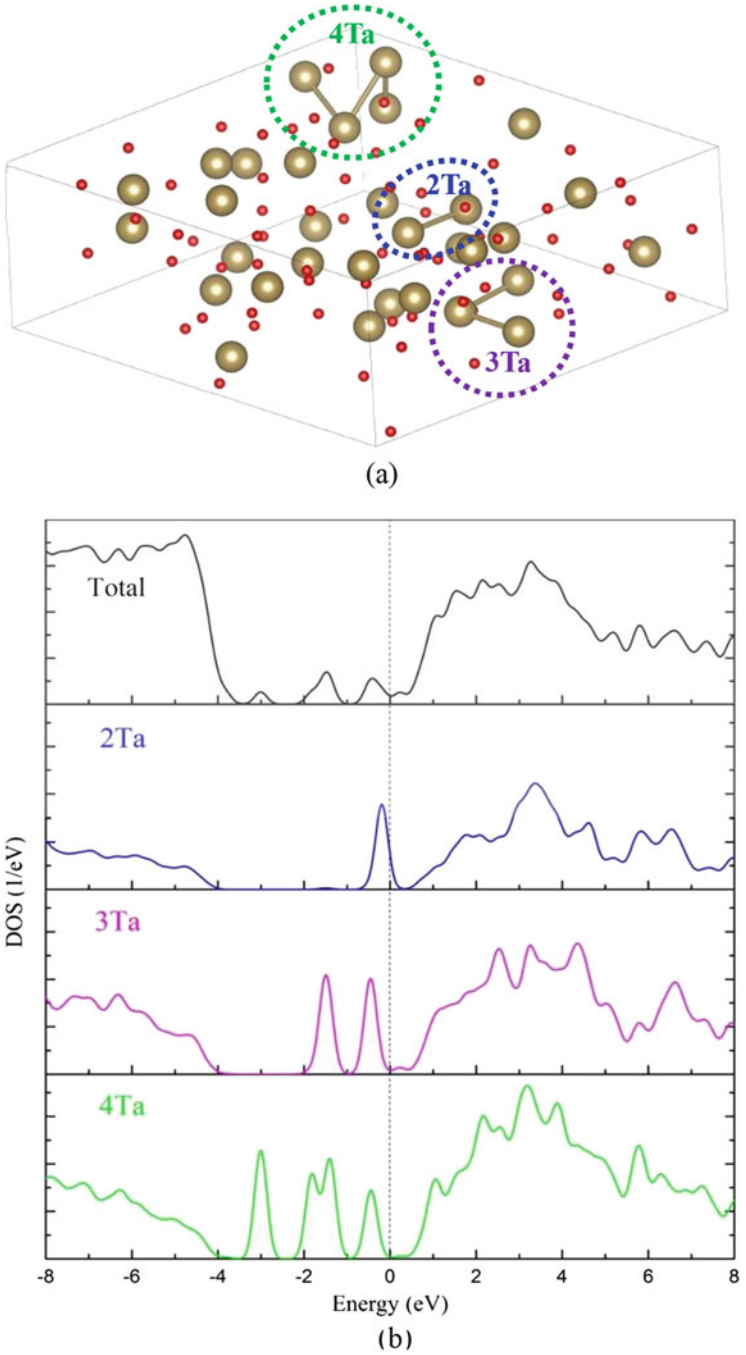


**Fig. 13** (**a**) Structure and (**b**) density of states of a-$TaO_{2.25}$

1073 K shows that the Ta dimer structures tend to merge into the Ta tetramer, which further confirms that the formation of Ta clusters is energetically preferable in the O-deficiency state of a-$Ta_2O_5$. This could be probably attributed to the simple equilibrium solid-phase diagram for the Ta-O system: there are only two stable phases below 1273 K: the single-metal-valence compound $Ta_2O_5$ and Ta metal [42].

Subsequently, in order to understand the structural evolution of Ta-O systems during operation, various a-$TaO_x$ (x = 2.85, 2.67, 2.50, 2.25, 2, 1.5, 1 and 0.75) structures were examined [7]. The values of Ta-O/Ta-Ta bond lengths and Ta(O)/O (Ta) coordination numbers (CNs) as the function of O contents are shown in Fig. 14a,b, respectively. Note that Ta(O) CN denotes the number of O atoms surrounding a Ta atom. From the figure, we can see that: (1) with the increase of x values, the Ta-O bond length gradually decreases; (2) the Ta(O) CN values increase with the increase of x values until it keeps almost a constant value (corresponding to $TaO_6$) in the region of $x > 2.50$. All the above features agree well with experimental data [43], supporting the reliability of our simulation results. In addition, other features of the structural evolution can also be seen: (3) the O(Ta) CN increases with the increase of $V_O$ concentrations; (4) there is the close relationship between the O(Ta) CN and Ta-O bond length, and between the Ta(O) CN and Ta-Ta bond length; (5) considerable amount of Ta-Ta metallic bonds are formed in the case of O-deficient a-$TaO_x$, which could dramatically enhance the electronic conductivity of a-$TaO_x$ and corresponds to LRS of the a-$TaO_x$ based device [5, 28].

To understand the correlation between electronic properties of a-$TaO_x$ and O contents, the calculated DOS of all the considered a-$TaO_x$(x = 2.85, 2.67, 2.50, 2.25, 2, 1.5, 1 and 0.75) are shown in Fig. 15. This figure reveals that: (1) in the case of a-$TaO_x$ with $x > 2.50$, the defect states near the Fermi level mainly consist of the O-O bonds [43]; (2) a-$TaO_{2.5}$ is an insulator with a big band gap; (3) in the case of a-$TaO_x$ with $x < 2.50$, the Fermi level shift towards the conduction band due to the formation of Ta-Ta bonds, and the intensity of defect states around the Fermi level becomes stronger with the decrease of O content concentration.

As revealed in the previous experiment [28], the chemical compositions of Ta-O system for HRS and LRS in a-$TaO_x$ based device correspond to the values $x > 2$ and $x < 1$, respectively. Accordingly, we chose the a-$TaO_{2.25}$ and a-$TaO_{0.75}$ to represent of the HRS and LRS, respectively, and studied their structures and electronic properties in detail (Fig. 16). In the case of a-$TaO_{2.25}$, several Ta clusters can be found which are apart from each other, and the corresponding local density of states (LDOS) around the Fermi level (Fig. 16a) shows that the electrons are localized on these Ta clusters. Accordingly, no connected conduction path is formed. It is noted that the isolated Ta-rich regions were observed in the experiment in the HRS of a-$TaO_x$ based device [4]. On the other hand, in a-$TaO_{0.75}$ (Fig. 16b), a considerable amount of Ta-Ta bonds can be found which are connected with each other. The corresponding LDOS (Fig. 16b) reveals that electrons are delocalized on these Ta-Ta bonds, which results in the formation of conduction path. The results agree well with experiments showing the formation of a connected Ta-rich region in LRS of such device [4, 28]. In addition, the volume of a-$TaO_{2.25}$ structure is about twice of a-$TaO_{0.75}$, which agree with the experimental finding that the thickness of a-$TaO_x$

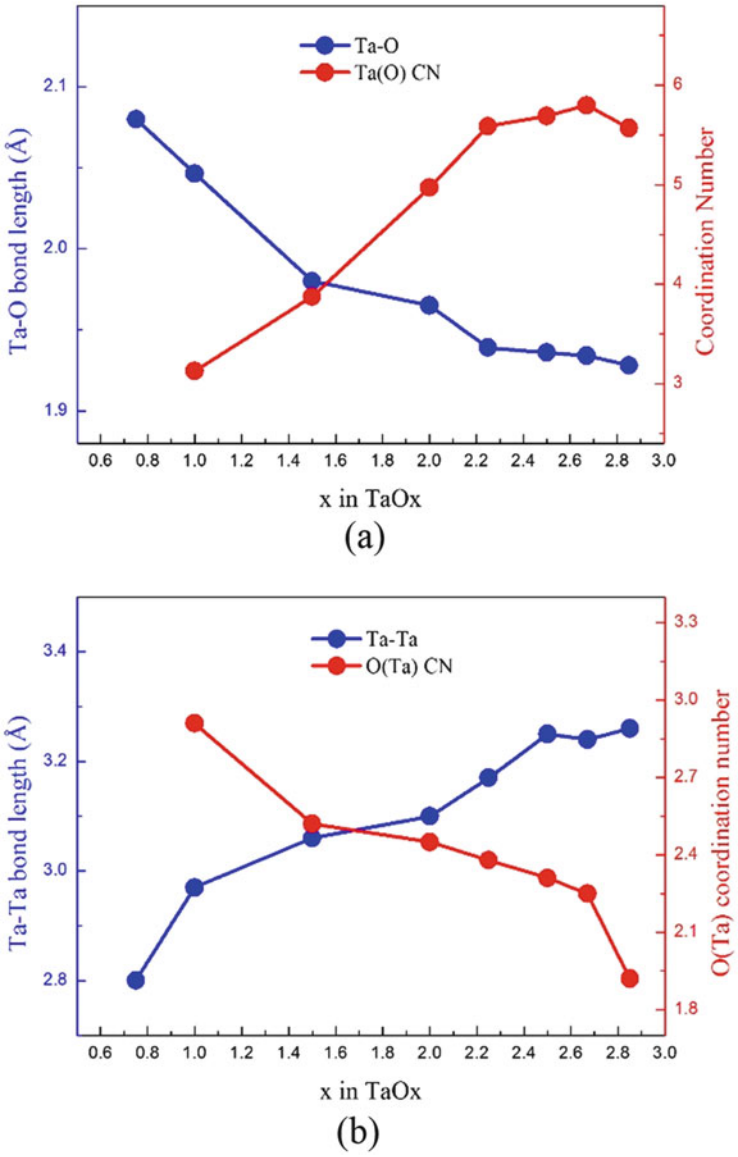


**Fig. 14** Changes of Ta-O/Ta-Ta bond lengths and Ta(O)/O(Ta) CNs dependent on x value in a-$TaO_x$. Adapted from Ref. [7] with permission from The Royal Society of Chemistry

was decreased by half after the electrical operations [37]. On the basis of these results, we conclude that the formation of Ta-Ta bonds, but not $V_O$s, is responsible for the LRS in a-$TaO_x$ based resistive switch.

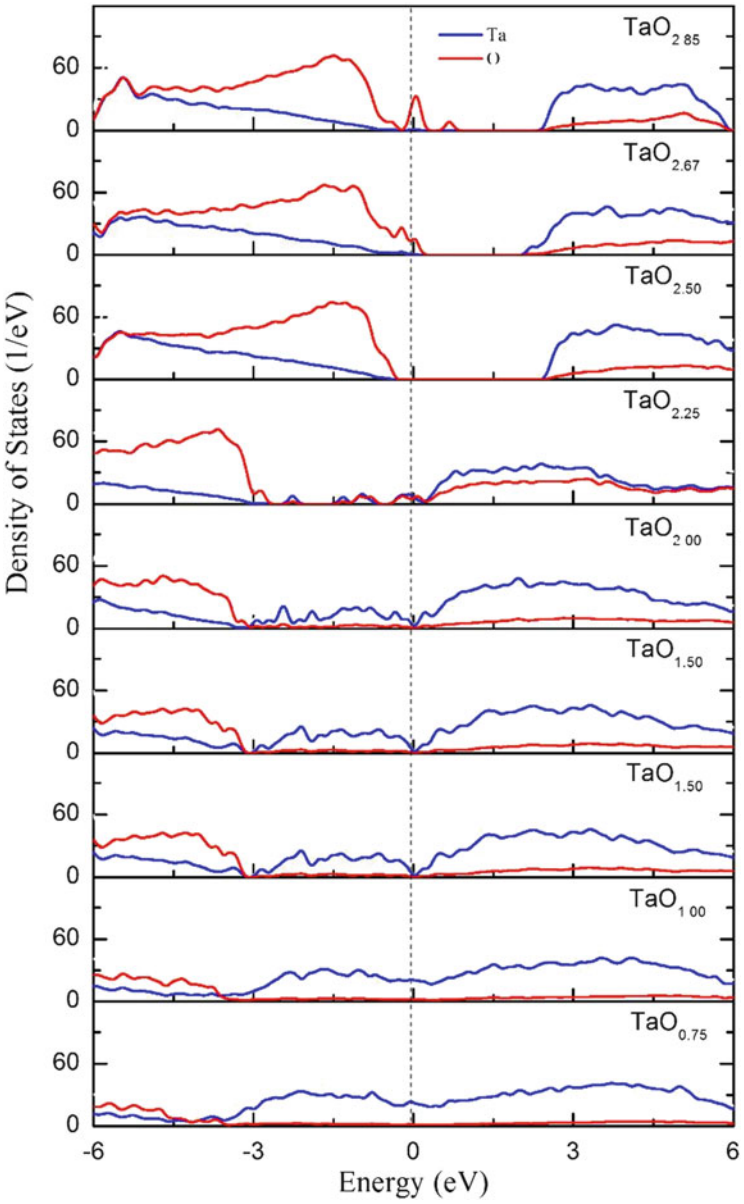


**Fig. 15** DOS of various a-$TaO_x$. Adapted from Ref. [7] with permission from The Royal Society of Chemistry

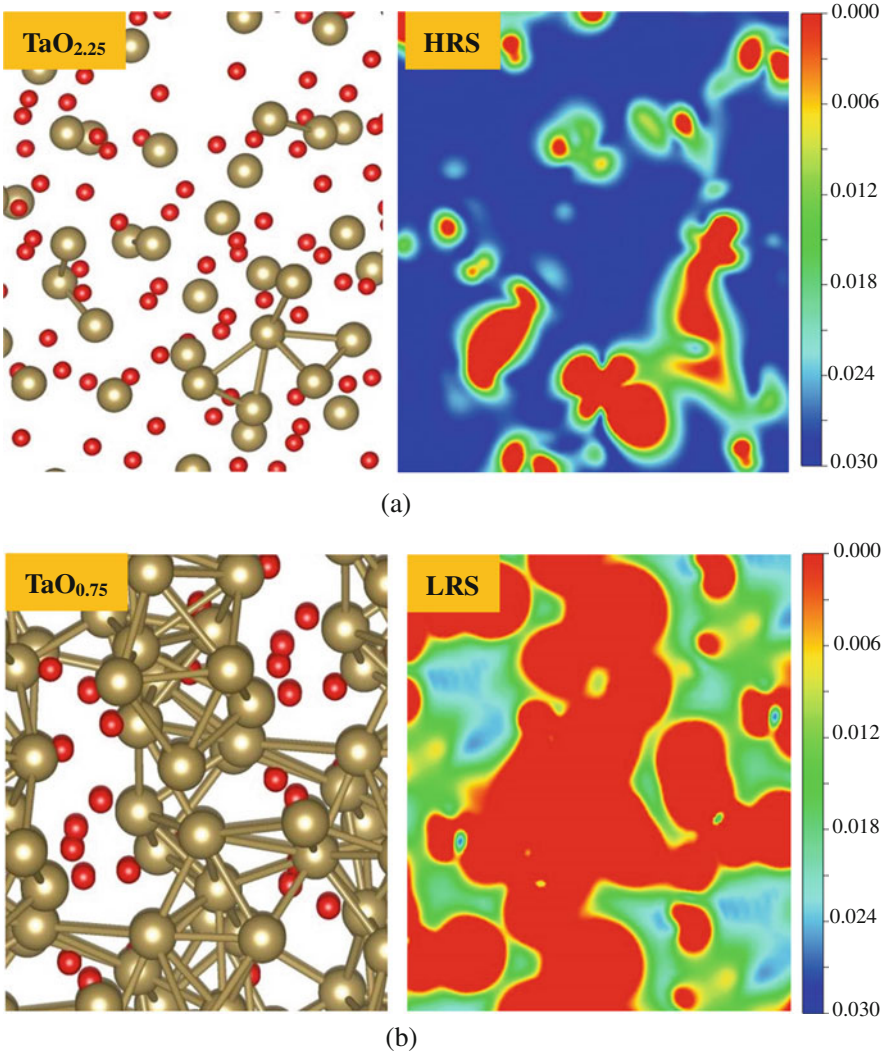


**Fig. 16** Structure and local density of states near the Fermi level of a-$TaO_{2.25}$ and a-$TaO_{0.75}$, respectively. Adapted from Ref. [7] with permission from The Royal Society of Chemistry

### 4.1.3 Crystallization of Conduction Path in a-$TaO_x$ Based Resistive Switch

Even though the Ta-rich region in CF of a-$TaO_x$-based resistive switch had been identified in experiment, its atomic detail was still unknown due to the experimental limitations. Therefore we examined the structure of CF (a-$TaO_{0.75}$) on atomic level from theoretical point of view [7]. As shown in Fig. 17, the atomic arrangement in

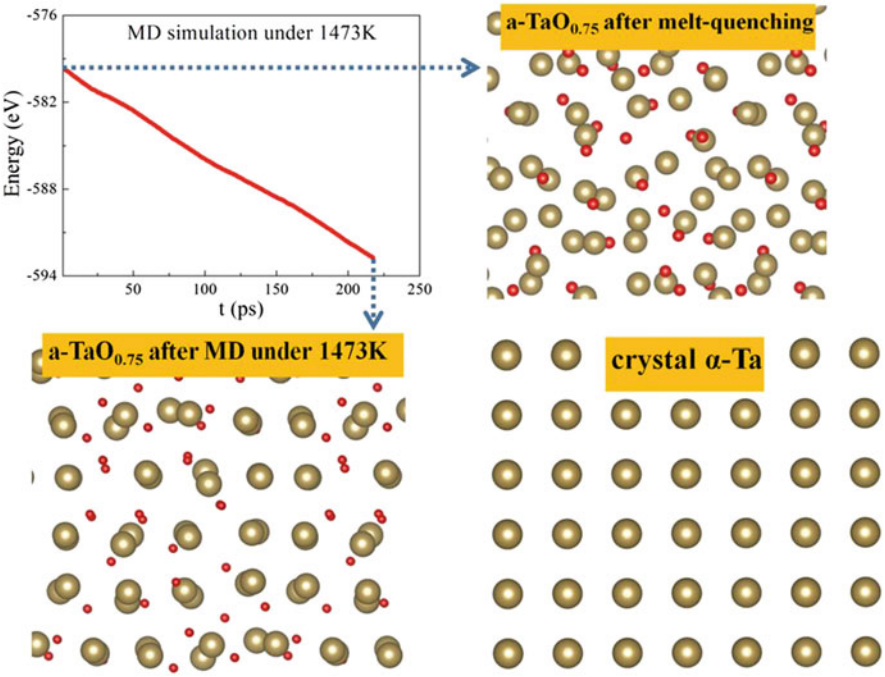


**Fig. 17** Change of a-$TaO_{0.75}$ structure during MD simulation. Structure of α-Ta is shown for comparison. Adapted from Ref. [7] with permission from The Royal Society of Chemistry

the a-$TaO_{0.75}$ structure generated by the melt-quenching method is disordered (Fig. 17). However, it becomes ordered after the MD simulation at 1473 K, accompanied by the decrease of the total energy. As can be seen in Fig. 17, the arrangement of Ta atoms in such ordered structure is similar to that of the crystalline α-Ta, which is the most stable phase of Ta [44]. In order to further explore the relationship between the a-$TaO_{0.75}$ and crystalline α-Ta, the structure relaxation was performed after removing all the O atoms in a-$TaO_{0.75}$. As expected, the generated structure is identical to the crystal α-Ta, and thus the structure of a-$TaO_{0.75}$ can be viewed as the α-Ta with interstitial O atoms. On the Basis of these results, we propose that the phase transition from a-$TaO_{0.75}$ to α-Ta with interstitial O atoms is likely to occur at high temperature.

In real devices, the CF region is considered to become very hot (from 873 K to 1633 K) during the electrical operation probably due to Joule heating. Furthermore, the crystallization of CF in a-$TaO_x$-based resistive switch has been observed during a long time electrical operation on LRS [28, 29], which supports our results.

### 4.1.4 Transport Property of Pt/a-TaO$_x$/Pt Resistive Switch

Next, we discuss the electron transport in the Pt/a-TaO$_x$/Pt device [7]. To examine this, we first constructed a Pt/a-TaO$_{2.5}$/Pt structure (Fig. 18a): the a-TaO$_{2.5}$ with 16.5 Å thick was generated by melt-quenching method, and then the structural optimization and MD simulation were carried out on the a-TaO$_{2.5}$ with including the Pt layers. The transmission spectrum for the Pt/a-TaO$_{2.5}$/Pt heterostructure shown in Fig. 18b reveals the poor electron conductivity due to the insulating nature of a-Ta$_2$O$_5$. On the other hand, in the case of the Pt/a-TaO$_{2.5-x}$/Pt structure, generation of discontinued Ta-rich regions between the two electrodes were detected by visual inspection (note that the O-deficient models were generated by removing oxygen atoms that were located near other oxygen atoms). As seen in Fig. 18b, small amount of defect states appear around the Fermi level, which results in the increased conduction (to ~0.03 in the unit of quantized conductance, 2e$^2$/h) in this system compared with the stoichiometric case. For the system with a continued CF (Pt/a-TaO$_{2-x}$/Pt), the value of transmission is about 0.6. It is worth noting that the on/off ratio of 20 in our calculation is comparable to that in a real device (~10) [4].

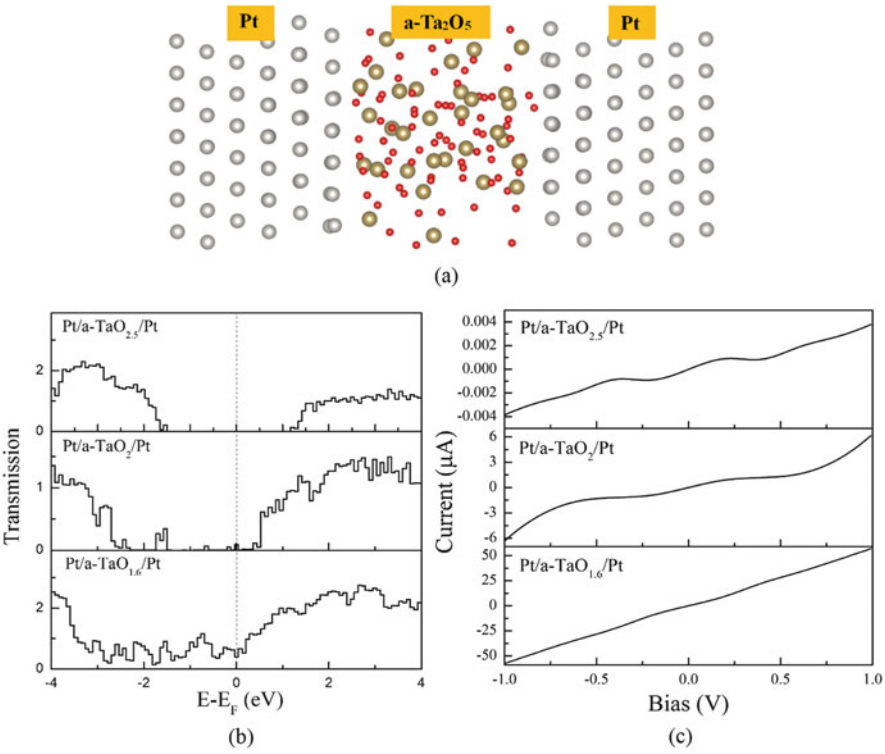


**Fig. 18** (**a**) Structure of Pt/a-Ta$_2$O$_5$/Pt, (**b**) transmission spectra and (**c**) current-voltage curves of the Pt/a-TaO$_x$/Pt. Adapted from Ref. [7] with permission from The Royal Society of Chemistry

Next, we calculated the current-voltage (I-V) curves of these three heterostructures, which are shown in Fig. 18c. The results further confirm the above features of conduction seen in the transmission spectra. For example, at the bias voltage of 1.0 V, a much larger current (~57 μA) flows in the heterostructure with a continued CF, as compared to the case with a discontinued CF (6 μA). The current value (~57 μA) is comparable to that in the real device [4], though this agreement may be accidental.

In summary of this subsection, the structures and electronic properties of a-$TaO_x$ (x = 2.85, 2.67, 2.50, 2.25, 2, 1.5, 1 and 0.75) were examined via first-principles calculations. Our results reveal that there is a strong correlation between the Ta (O) coordination number and the O-Ta (Ta-Ta) bond length. More importantly, we suggested that the formation of Ta-Ta bonding structures, but not $V_O$, is mainly responsible for the LRS in the Pt/a-$TaO_x$/Pt resistive switches.

## 4.2 *Diffusion of Metal and Oxygen Ions in a-$TaO_x$ Based Resistive Switch*

Almost all the models proposed so far for the switching mechanism of a-$TaO_x$-based atomic switches are based on the diffusion of O ions or vacancies in a-$TaO_x$ [45]. Very recently, it was reported that the diffusion of Ta ions could also play an important role in the switching process of a-$TaO_x$-based resistive switches [46]. It should be noted that the diffusion of both Ta and O ions have already been observed during the growth of a-$TaO_x$ (x < 2.5) film [47, 48]. However, details of the behaviors of Ta and O ion diffusion in a-$TaO_x$ during the switching process are still unclear. Thus, to deepen the understanding on the switching mechanism of a-$TaO_x$-based resistive switches, we performed atomistic simulations to clarify the diffusion behaviors of both Ta and O ions during the switching processes [10].

### 4.2.1 Diffusion Coefficients and Barriers of Ta and O Ions in a-$TaO_x$

To examine the diffusion behaviors of Ta and O ions in a-$TaO_x$ (x = 2, 1.5 and 1), we calculated the time-average mean square displacement (MSD) at the temperatures of 873 K, 1073 K, 1273 K, 1473 K and 1673 K. From the time evolution of MSDs of Ta and O ions, we extracted the corresponding diffusion coefficients (D). Then from the temperature dependence of D shown in Fig. 19, we have evaluated the activation energies ($E_a$) according to Arrhenius equation. Our results revealed that D and $E_a$ of Ta and O ions have strong correlation with the O concentration in a-$TaO_x$: D ($E_a$) values of Ta and O ions increase (decrease) with the decrease of O content in a-$TaO_x$.

Our calculated values of $E_a$ for O ions in a-$TaO_x$ (x = 2, 1.5 and 1) are 0.59, 0.41 and 0.31 eV, respectively, which agrees with the experimental results (from 0.29 to

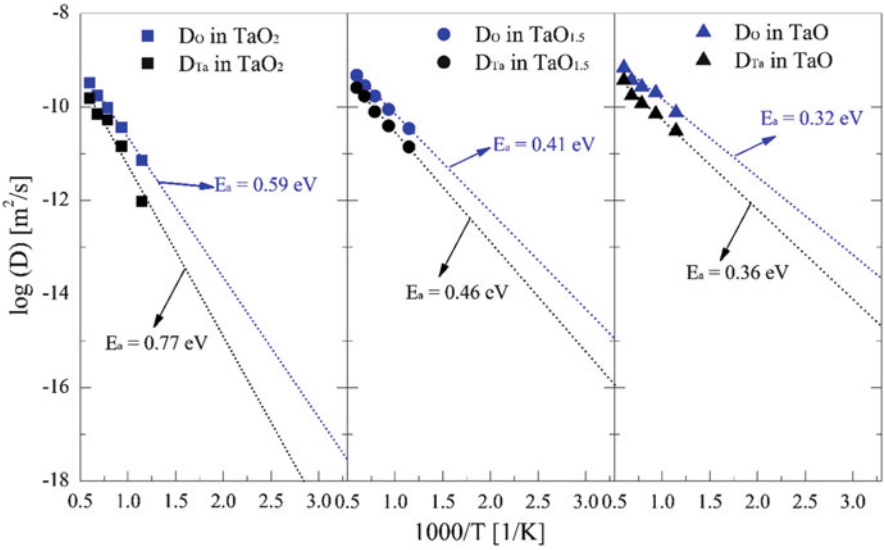


**Fig. 19** Diffusion coefficients and energy barriers of Ta and O ions in a-$TaO_x$ with various O concentrations. Adapted from Ref. [10] with permission from American Chemical Society

0.45 eV) [49]. As can be seen in Fig. 19, the values of D of Ta ions ($D_{Ta}$) are always smaller than those of O ions in a-$TaO_x$ irrespective of the O contents. Interestingly, as the O vacancy concentration increases, $D_{Ta}$ approaches to $D_O$, which means that the diffusion of Ta is more significant in the conductive filament (O-poor region) than in the O-rich region.

As mentioned in the previous experiment [50], in the LRS of the a-$TaO_x$-based atomic switches, the CF is composed of a-TaO. During the switching process, the local temperature of filament rises sharply due to the Joule heating, especially during the RESET process in the bipolar device (from 300 to 600 K) and unipolar device (from 300 to 1200 K) [51–53]. As seen in Fig. 19, $D_{Ta}$ in a-TaO is four times smaller than $D_O$ at 300 K, but the ratio is reduced to 2 at 1200 K. Our results agree with the experimental observation that $D_{Ta}$ is two to three times lower than $D_O$ during the growth of a-$TaO_x$ [47]. On the basis of these results, we can say that the diffusion of Ta ions is non-negligible in the CF, and thus responsible for the switching of a-$TaO_x$-based atomic switches, especially for unipolar switching. It is noted that the value of $D_{Ta}$ in a-$TaO_{1.5}$ is only three to ten times smaller than $D_O$ in the temperature range from 300 to 1200, which suggests that the diffusion of Ta ions may occur during the whole switching process of a-$TaO_x$-based devices.

On the basis of the above, we proposed a schematic model to explain the switching process of a-$TaO_x$ based devices [10], that is, the diffusion of O ions is predominant in the initial forming process of a-$TaO_x$; as the O concentration decreases, the Ta ion diffusion becomes relatively more significant, especially in the LRS region.

### 4.2.2 Diffusion Mechanism of Ta and O Ions in a-$TaO_x$

To deepen our understanding on the diffusion behaviors of Ta and O ions in a-$TaO_x$, here we discuss them in the light of the dependence of the structural parameters (such as CN and bond length) on x value of a-$TaO_x$ (x = 2.85, 2.67, 2.50, 2.25, 2, 1.5, 1 and 0.75) [10]. The x dependence of the Ta-O bond lengths and CNs, both Ta (O) and O(Ta), are plotted in Fig. 14. The results show that the Ta-O bond length increases with the decrease of x, which expands the free atomic volume around both metal (Ta) and O atoms, and consequently enhances their mobility. In particular, the CN of O(Ta) increases by ~1 as x decreases from 2.85 to 0.75 as seen in Fig. 14. This corresponds to the change of the component unit from $OTa_2$ to $OTa_3$, and as a result suppresses the mobility of O ions in some degree due to the increased steric hindrance around themselves. In contrast, the CN of Ta(O) shows obvious decrease (by ~3) with the decrease of x as seen in Fig. 14. This corresponds to the change of the component unit from octahedral $TaO_6$ to $TaO_3$, and will dramatically enhance the mobility of Ta ions due to the decreased steric hindrance around themselves. Thus, the enhancement of Ta ion mobility in a-$TaO_x$ is more obvious than that of O ions as the decrease of O concentration, and consequently the mobility of Ta and O ions is close to each other under low O concentration.

It is noted that our theoretical results agree with the previous experiments on the growth of $TaO_x$ ($x < 2.5$), which shows that the diffusion of Ta ions in a-$TaO_x$ layer is non-negligible [47]. Accordingly, from the diffusion behaviors of metal ions during the growth of metal oxide films, we may be able to obtain useful information to understand the switching mechanism of metal oxide based resistive switches. In experiments, the metal ion diffusion has already been observed in metal sub-oxide layer during oxide film growth for Ti, Al, Nb and W [47]. On the basis of these results, we can speculate that the metal ion diffusion in $TaO_x$, $TiO_x$, $AlO_x$, $NbO_x$ and $WO_x$ could occur during the switching of resistive switches based on these materials.

In summary of this subsection, we investigated the diffusion behavior of Ta and O ions in a-$TaO_x$ with various O concentrations. Our results reveal that the diffusion of Ta ions is enhanced with the decrease of O concentration, and approaches to that of O ions at the extremely low O concentration cases. Such phenomenon can be attributed to the combined effect of the changes in the Ta/O coordination numbers and the Ta-O/Ta-Ta bond strengths with the charge of O concentration in a-$TaO_x$.

## 5 Concluding Remarks

In this chapter, we have discussed several issues related to the switching mechanism of amorphous $TaO_x$ (a-$TaO_x$) based resistive switches on the basis of our simulations within the density functional theory. Our results reveal that (1) Cu nanowires with a diameter of three atoms or larger can work as conduction filaments (CFs) in the Cu/a-$Ta_2O_5$/Pt atomic switch; (2) Cu atoms tend to be ionized at the Cu/a-$Ta_2O_5$ interface,

and the ionization behavior becomes obvious with the increase of interface O concentration and/or temperature; (3) the CF in the Pt/a-$TaO_x$/Pt resistive switch consists of Ta-Ta bonding structures, but not O vacancies; (4) the mobility of Ta ions in the CF region of Pt/a-$TaO_x$/Pt device is comparable to that of O ions, and thus could actively participate in the switching process of a-$TaO_x$ based devices.

For the atomistic understanding on the switching mechanism of the (a-$TaO_x$) based resistive switches, several issues still remain as future tasks. For example, the atomistic details on the effects of moisture on the Cu diffusion [5] have not been clarified yet. In fact, our preliminary simulation, where we compared the Cu diffusion behaviors between bare and water-adsorbed a-$Ta_2O_5$ surfaces, suggests that the Cu diffusion can be faster on the water-adsorbed surface than the bare one [11]. Theoretical studies based on a more realistic model, however, would be desirable.

For tackling with such issues, density functional calculations are still heavy even on the current supercomputers. So development of methods that have both reliability and computational efficiency is highly desired. For this purpose, the interatomic potentials constructed by combining the density functional calculations and machine-learning techniques have attracted much attention recently. We applied such approaches to Cu diffusion in the a-$Ta_2O_5$ [54] and Li diffusion in a-$Li_3PO_4$ [55], but extensive investigation using these approaches remains as a future task.

**Acknowledgments** We thank Prof. Tinkun Gu, Prof. Tomofumi Tada for collaboration in the early stage of the present work. SW also thanks Prof. Shu Yamaguchi, Prof. Tsuyoshi Hasegawa, Dr. Tohru Tsuruoka, Dr Toshi Sakamoto and Dr Naoki Banno for fruitful discussion. This work was partially supported by CREST-JST "Atom transistor", Low Power Electronics Association and Projects, the grant-in-aid for Innovation Area "Computics" by MEXT, Japan, and Global COE program "Global COE for Mechanical Systems Innovation" by MEXT, Japan.

## References

1. Wang, J.Y., Li, L.Z., Huyan, H., Pan, X.Q., Nonnenmann, S.: Highly uniform resistive switching in $HfO_2$ films embedded with ordered metal nanoisland arrays. Adv. Funct. Mater. **29**, 1808430 (2019)
2. Zhou, G.D., Duan, S.K., Li, P., Sun, B., Wu, B., Yao, Y.Q., Yang, X.D., Han, J.J., Wu, J.G., Wang, G., Liao, L.P., Lin, C.Y., Hu, W., Xu, C.Y., Liu, D.B., Chen, T., Chen, L.J., Zhou, A.K., Song, Q.L.: Coexistence of negative differential resistance and resistive switching memory at room temperature in $TiO_x$ modulated by moisture. Adv. Electron. Mater. **4**, 1700567 (2018)
3. Prakash, A., Jana, D., Maikap, S.: $TaO_x$-based resistive switching memories: Prospective and challenges. Nanoscale Res. Lett. **8**, 418 (2013)
4. Lee, M.J., Lee, C.B., Lee, D., Lee, S.R., Chang, M., Hur, J.H., Kim, Y.B., Kim, C.J., Seo, D.H., Seo, S., Chung, U., Kim, K.: A fast, high-endurance and scalable non-volatile memory device made from asymmetric $Ta_2O_{5-x}$/$TaO_{2-x}$ bilayer structures. Nat. Mater. **10**, 625–630 (2011)
5. Valov, L., Tsuruoka, T.: Effects of moisture and redox reactions in VCM and ECM resistive switching memories. J. Phys. D. Appl. Phys. **51**, 413001 (2018)
6. Xiao, B., Gu, T.K., Tada, T., Watanabe, S.: Conduction paths in Cu/amorphous- $Ta_2O_5$/Pt atomic switch: First-principles studies. J. Appl. Phys. **115**, 034503 (2014)

7. Xiao, B., Watanabe, S.: Oxygen vacancy effects on an amorphous-$TaO_x$-based resistance switch: A first principles study. Nanoscale. **6**, 10169–10178 (2014)
8. Xiao, B., Watanabe, S.: Interface structure in Cu/$Ta_2O_5$/Pt resistance switch: A first-principles study. ACS Appl. Mater. Interfaces. **7**, 519–525 (2015)
9. Xiao, B., Yu, X.F., Cheng, J.B.: Atomic insight into the origin of various operation voltages of cation-based resistance switches. ACS Appl. Mater. Interfaces. **8**, 31978–31985 (2016)
10. Xiao, B., Yu, X.F., Watanabe, S.: A comparative study on the diffusion behaviors of metal and oxygen ions in metal-oxide-based resistance switches via ab initio molecular dynamics simulations. ACS Appl. Electron. Mater. **1**, 585–549 (2019)
11. Xiao, B., Watanabe, S.: Moisture effect on the diffusion of Cu ions in Cu/$Ta_2O_5$/Pt and Cu/$SiO_2$/Pt resistances switches: A first-principle study. Sci. Technol. Adv. Mat. **20**, 580–588 (2019). https://doi.org/10.1080/14686996.2019.1616222
12. Kresse, G., Furthmüller, J.: Efficiency of ab-initio total energy calculations for metals and semiconductors using a plane-wave basis set. Comput. Mater. Sci. **6**, 15–50 (1996)
13. Kresse, G., Furthmüller, J.: Efficient iterative schemes for ab initio total-energy calculations using a plane-wave basis set. Phys. Rev. B. **54**, 11169 (1996)
14. Kresse, G., Joubert, J.: From ultrasoft pseudopotentials to the projector augmented-wave method. Phys. Rev. B. **59**, 1758 (1999)
15. Wang, Y., Perdew, J.P.: Correlation hole of the spin-polarized electron gas, with exact small-wave-vector and high-density scaling. Phys. Rev. B. **44**, 13298 (1991)
16. Brandbyge, M., Mozos, J., Ordejon, P., Taylor, J., Stokbro, K.: Density-functional method for nonequilibrium electron transport. Phys. Rev. B. **65**, 165401 (2002)
17. Terabe, K., Hasegawa, T., Nakayama, T., Aono, M.: Quantized conductance atomic switch. Nature. **433**, 47–50 (2005)
18. Waser, R., Aono, M.: Nanoionics-based resistive switching memories. Nat. Mater. **6**, 833–840 (2007)
19. Sawa, A.: Resistive switching in transition metal oxides. Mater. Today. **11**, 28–36 (2008)
20. Gu, T.K., Wang, Z.C., Tada, T., Watanabe, S.: First-principles simulations on bulk $Ta_2O_5$ and Cu/$Ta_2O_5$/Pt heterojunction: Electronic structures and transport properties. J. Appl. Phys. **106**, 103713 (2009)
21. Gu, T.K., Tada, T., Watanabe, S.: Conductive path formation in the Ta2O5 atomic switch: First-principles analyses. ACS Nano. **4**, 6477–6482 (2010)
22. Kim, M.J., Seo, Y., Cruz, M.A., Wiley, B.J.: Metal nanowire felt as a flow-through electrode for high-productivity electrochemistry. ACS Nano. **13**, 6998–7009 (2019). https://doi.org/10.1021/acsnano.9b02058
23. Gonzalez, J.C., Rodrigues, V., Bettini, J., Rego, L.G.C., Rocha, A.R., Coura, P.Z., Dantas, S. O., Sato, F., Galvao, D.S., Ugarte, D.: Indication of unusual pentagonal structures in atomic-size Cu nanowires. Phys. Rev. Lett. **93**, 126103 (2004)
24. Zhou, Z., Zhao, J.J., Chen, Z.F., Gao, X.P., Lu, J.P., Schleyer, P.V.R., Yang, C.K.: True nanocable assemblies with insulating BN nanotube sheaths and conducting Cu nanowire cores. J. Phys. Chem. B. **110**, 2529–2532 (2006)
25. Banno, N., Sakamoto, T., Iguchi, N., Matsumoto, M., Imai, H., Ichihashi, T., Fujieda, S., Tanaka, K., Watanabe, S., Yamaguchi, S., Hasegawa, T., Aono, M.: Structural characterization of amorphous $Ta_2O_5$ and $SO_2$-$Ta_2O_5$used as solid electrolyte for nonvolatile switches. Appl. Phys. Lett. **97**, 113507 (2010)
26. Lee, S., Kim, J., Kim, S., Kim, S., Park, G.: Hidden structural order in orthorhombic. Phys. Rev. Lett. **110**, 235502 (2013)
27. KC, S., Dong, H., Longo, R.C., Wang, W.C., Xiong, K., Wallace, R.M., Cho, K.: Electronic properties of InP (001)/$HfO_2$ (001) interface: Band offsets and oxygen dependence. J. Appl. Phys. **115**, 023703 (2014)
28. Park, G.S., Kim, Y.B., Park, S.Y., Li, X.S., Heo, S., Lee, M.J., Chang, M., Kwon, J.H., Kim, M., Chung, U.I., Dittmann, R., Waser, R., Kim, K.: In situ observation of filamentary

conducting channels in an asymmetric $Ta_2O_{5-x}/TaO_{2-x}$ bilayer structure. Nat. Commun. **4**, 2382 (2013)
29. Miao, F., Strachan, J.P., Yang, J.J., Zhang, M.X., Goldfarb, I., Torrezan, A.C., Eschbach, P., Kelley, R.D., Medeiros-Ribeiro, G., Williams, R.S.: Anatomy of a nanoscale conduction channel reveals the mechanism of a high-performance memristor. Adv. Mater. **23**, 5633–5640 (2011)
30. Jagath, A.L., Kumar, T.N., Almurib, H.A. Modeling of current conduction during RESET phase of $Pt/Ta_2O_5/TaO_x/Pt$ bipolar resistive RAM devices. In: IEEE 7th Non-Volatile Memory Systems and Applications Symposium (NVMSA). (2018). https://doi.org/10.1109/NVMSA.2018.00014
31. Yang, J.J., Kobayashi, N.P., Strachan, J.P., Zhang, M.X., Ohlberg, D.A.A., Pickett, M.D., Li, Z., Medeiros-Ribeiro, G., Williams, R.S.: Dopant control by atomic layer deposition in oxide films for memristive switches. Chem. Mater. **23**, 123–125 (2011)
32. Yang, J.J., Strachan, J.P., Miao, F., Zhang, M.X., Pickett, M., Yi, W., Ohlberg, D., Medeiros-Ribeiro, G., Williams, R.: Metal/$TiO_2$ interfaces for memristive switches. Appl. Phys. A Mater. Sci. Process. **102**, 785–789 (2011)
33. Xu, N., Gao, B., Liu, L.F., Sun, B., Liu, X.Y., Han, R.Q., Kang, J.F., Yu, B.: A unified physical model of switching behavior in oxide-based RRAM. Symposium on VLSI Technology Digest of technical papers, pp. 100–101 (2008)
34. Hur, J.H., Lee, M.J., Lee, C.B., Kim, Y.B., Kim, C.J.: Modeling for bipolar resistive memory switching in transition-metal oxides. Phys. Rev. B. **82**, 155321 (2010)
35. Wei, Z., Takagi, T., Kanzawa, Y., Katoh, Y., Ninomiya, T., Kawai, K., Muraoka, S., Mitani, S., Katayama, K., Fujii, S., Miyanaga, R., Kawashima, Y., Mikawa, T., Shimakawa, K., Aono, K.: Demonstration of high-DENSITY ReRAM ensuring 10-year retention at 85°C. Based on a newly developed reliability model. IEDM11–721, 31.4.1–31.1.4 (2011)
36. Choi, S., Yang, Y.C., Lu, W.: Random telegraph noise and resistance switching analysis of oxide based resistive memory. Nanoscale. **7**, 400–404 (2014)
37. Yang, J.J., Zhang, M.X., Strachan, J.P., Miao, F., Pickett, M.D., Kelley, R.D., Medeiros-Ribeiro, G., Williams, R.S.: High switching endurance in $TaO_x$ memristive devices. Appl. Phys. Lett. **97**, 232102 (2010)
38. Heyd, J., Scuseria, G.E., Ernzerhof, M.: Hybrid functionals based on a screened coulomb potential. J. Chem. Phys. **118**, 8207 (2003)
39. Lau, W.S., Leong, L.L., Han, T., Sandler, N.P.: Detection of oxygen vacancy defect states in capacitors with ultrathin $Ta_2O_5$ films by zero-bias thermally stimulated current spectroscopy. Appl. Phys. Lett. **83**, 2835 (2003)
40. Ivanov, M.V., Perevalov, T.V., Aliev, V.S., Gritsenko, V.A., Kaichev, V.V.: Effect of dielectric stoichiometry and interface chemical state on band alignment between tantalum oxide and platinum. J. Appl. Phys. **110**, 024115 (2011)
41. Lau, W.S.: Engineering implication of the correlation between the leakage current in high-k dielectric materials and the electronic defect states detected by zero-bias thermally simulated current spectroscopy. China Semiconductor Technology International Conference (CSTIC). (2018). https://doi.org/10.1109/CSTIC.2018.8369248
42. Garg, S.P., Krishnamurthy, N., Awasthi, A., Venkatraman, M.: The O-Ta (oxygen-tantalum) system. J. Phase Equilib. **17**, 63–77 (1996)
43. Alderman, O.L.G., Benmore, C.J., Neuefeind, J., Coillet, E., Mermet, A., Martinez, V., Tamalonis, A., Weber, R.: Amorphous tantala and its relationship with the molten state. Phys. Rev. Mater. **2**, 043602 (2018)
44. Jiang, A.Q., Tyson, T.A., Axe, L.: The structure of small Ta clusters. J. Phys. Condens. Matter. **17**, 1841 (2005)
45. Park, T.H., Kwon, Y.J., Kim, H.J., Woo, H.C., Kim, G.S., An, C.H., Kim, C.H., Kwon, D.E., Hwang, C.S.: Balancing the source and sink of oxygen vacancies for the resistive switching memory. ACS Appl. Mater. Interfaces. **10**, 21445–21450 (2018)

46. Wedig, A., Luebben, M., Cho, D.Y., Moors, M., Skaja, K., Rana, V., Hasegawa, T., Adepalli, K.K., Yildiz, B., Waser, R., Valov, L.: Nanoscale cation motion in $TaO_x$, $HfO_x$ and $TiO_x$ memristive systems. Nat. Nanotechnol. **11**, 67–74 (2016)
47. Davies, J.A., Domeij, B., Pringle, J.P.S., Brown, F.: The migration of metal and oxygen during anodic film formation. J. Electrochem. Soc. **112**, 675–680 (1965)
48. Khalil, N., Leach, J.S.L.: The anodic oxidation of valve metals—I. determination of ionic transport numbers by a-spectrometry. Electrochim. Acta. **31**, 1279–1285 (1986)
49. Chandrasekharan, R., Park, I., Masel, R.I., Shannon, M.A.: Thermal oxidation of tantalum films at various oxidation states from 300 to 700°C. J. Appl. Phys. **98**, 114908 (2005)
50. Oshima, M., Toyoda, S., Horiba, K., Yasuhara, R., Kumigashira, H.: Synchrotron radiation nano-spectroscopy of dielectrics for LSI and ReRAM. ECS Trans. **41**, 453 (2011)
51. Yang, J.J., Strukov, D.B., Stewart, D.R.: Memristive devices for computing. Nat. Nanotechnol. **8**, 13–24 (2013)
52. Yalon, E., Gavrilov, A., Cohen, S., Ritter, D.: Validation and extension of local temperature evaluation of conductive filaments in RRAM devices. IEEE Trans. Electron Devices. **62**, 3671–3677 (2015)
53. Sharma, A.A., Noman, M., Abdelmoula, M., Skowronski, M., Bain, J.A.: Electronic instabilities leading to electroformation of binary metal oxide-based resistive switches. Adv. Funct. Mater. **24**, 5522–5529 (2014)
54. Li, W., Ando, Y., Watanabe, S.: Cu diffusion in amorphous $Ta_2O_5$ studied with a simplified neural network potential. J. Phys. Soc. Jpn. **86**, 104004 (2017)
55. Li, W., Ando, Y., Minamitani, E., Watanabe, S.: Study of Li atom diffusion in amorphous $Li_3PO_4$ with neural network potential. J. Chem. Phys. **147**, 214106 (2017)